Petrology of the regional sillimanite zone, west-central New Hampshire, U.S.A., with implications for the development of inverted isograds

FRANK S. SPEAR
Department of Earth and Environmental Sciences, Rensselaer Polytechnic Institute, Troy, New York 12180, U.S.A.

MATTHEW J. KOHN
Department of Geology and Geophysics, University of Wisconsin, Madison, Wisconsin 53706, U.S.A.

STEPHAN PAETZOLD
Department of Earth and Environmental Sciences, Rensselaer Polytechnic Institute, Troy, New York 12180, U.S.A.

ABSTRACT

Sillimanite from the regional sillimanite zone in west-central New Hampshire is fibrolitic and overprints F_2 folds (nappe stage) of earlier mica foliation. Regional sillimanite zone samples show no evidence for earlier staurolite parageneses, despite the fact that staurolite is abundant at lower grade, because sillimanite was produced directly from garnet + chlorite by the prograde (heating) reaction garnet + chlorite + muscovite + quartz = sillimanite + biotite + H_2O. The pressure at which this reaction occurs is sensitive to the MnO and CaO contents of garnet, and phase-equilibrium arguments reveal that at the regional pressures of west-central New Hampshire (2–4 kbar), staurolite parageneses are only possible in rocks with low MnO + CaO.

The inferred P-T path is counterclockwise with nearly isobaric initial heating at 2 kbar, followed by loading (± heating) to a peak metamorphic temperature of 600 ± 25 °C at 4 kbar, followed by nearly isobaric cooling. Garnets were compositionally homogenized near the metamorphic peak, but subsequent cooling was rapid (>100 °C/m.y.). These data argue against the folded isotherm model of Chamberlain (1986). Instead, the present distribution of metamorphic grades is interpreted to be the result of regional stacking of high-grade thrust sheets on lower grade rocks, followed by depression of high-grade rocks to lower structural levels.

INTRODUCTION

The transition from the staurolite zone to the sillimanite zone along the eastern margin of the Bronson Hill anticlinorium, central New Hampshire, is quite abrupt, with little overlap between the two zones. Indeed, one of the most striking features is that there is no petrographic evidence in the sillimanite zone rocks that staurolite was a precursor to sillimanite parageneses.

Bulk composition differences provide the most likely explanation for this observation. Specifically, the sillimanite zone rocks are richer in Mn and have developed sillimanite parageneses directly from garnet + chlorite assemblages by the reaction

$$\text{garnet + chlorite + muscovite + quartz}$$
$$= \text{sillimanite + biotite + } H_2O. \qquad (1)$$
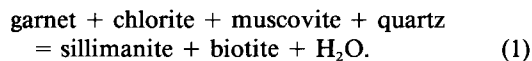
If this interpretation is correct, it places some important restrictions on the P-T path followed by the rocks and on the timing of mineral growth relative to fabric development and tectonic evolution.

The purpose of this paper is to present textural and compositional data on mineral assemblages in sillimanite-zone rocks. These are integrated with a theoretical analysis of the phase equilibria of these rocks and interpreted with respect to the rocks' P-T path.

GEOLOGIC SETTING

The Acadian structure of west-central New Hampshire is characterized by a series of thrust and fold nappes (the so-called nappe stage of deformation: e.g., the Skitchewaug, the Fall Mountain, and the Chesham Pond nappes) that are folded by broad, open folds, some of which are cored by gneiss domes (the so-called dome stage of deformation: e.g., the Alstead dome) (Fig. 1; Thompson et al., 1968; Thompson and Rosenfeld, 1979; Chamberlain, 1986). The Skitchewaug nappe is exposed over much of the central part of the study area and is best observed as a recumbent syncline at the northeast end of the Alstead dome in the central part of the map area (near sample 89-14). The Fall Mountain nappe is exposed as a klippe at Fall Mountain (samples BF-9, BF-14, BF-48) with the root zone in the vicinity of Gilsum. The Chesham Pond nappe occurs in the eastern part of the study area and is floored by the Chesham Pond thrust.

Deformation has produced two schistosities and a late kink banding. The earliest schistosity (S_1) is pervasively
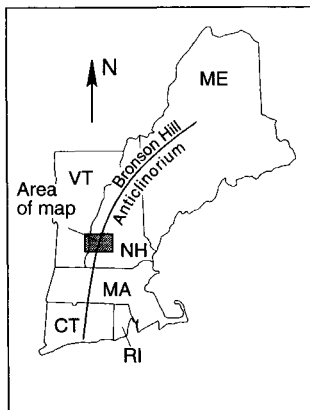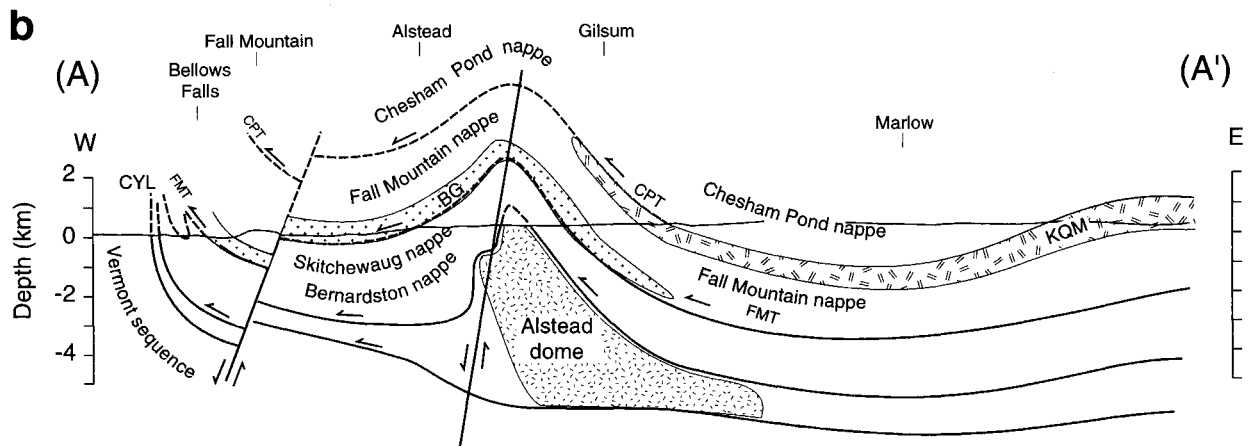
Fig. 1. (a) Geologic map and cross section of the study area in west-central New Hampshire and adjacent Vermont. BFP = Bellows Falls pluton; CYL = "chicken yard line"; AD = Alstead dome; CPT = Chesham Pond thrust; FMT = Fall Mountain thrust. Geology after Kruger (1946), Thompson et al. (1968), Thompson and Rosenfeld (1979), Chamberlain (1985), Allen (1984), and the authors' mapping. Squares = prismatic sillimanite after andalusite; inverted triangles = prismatic sillimanite within muscovite pseudomorphs; triangles = fibrolitic sillimanite within muscovite; circles = regional fibrolitic sillimanite; plus signs = staurolite zone samples. Numbers are sample locations. Isograds (Grt = garnet, St = staurolite + biotite, Sil = sillimanite + biotite + muscovite, Kfs = sillimanite + potassium feldspar, Crd = garnet + cordierite) delineate the occurrence of minerals in the field but are not all the same generation. Note that the staurolite isograd corresponds to a thrust surface. (b) Cross section shows stacking of nappe sequence and location of study area (no vertical exaggeration).
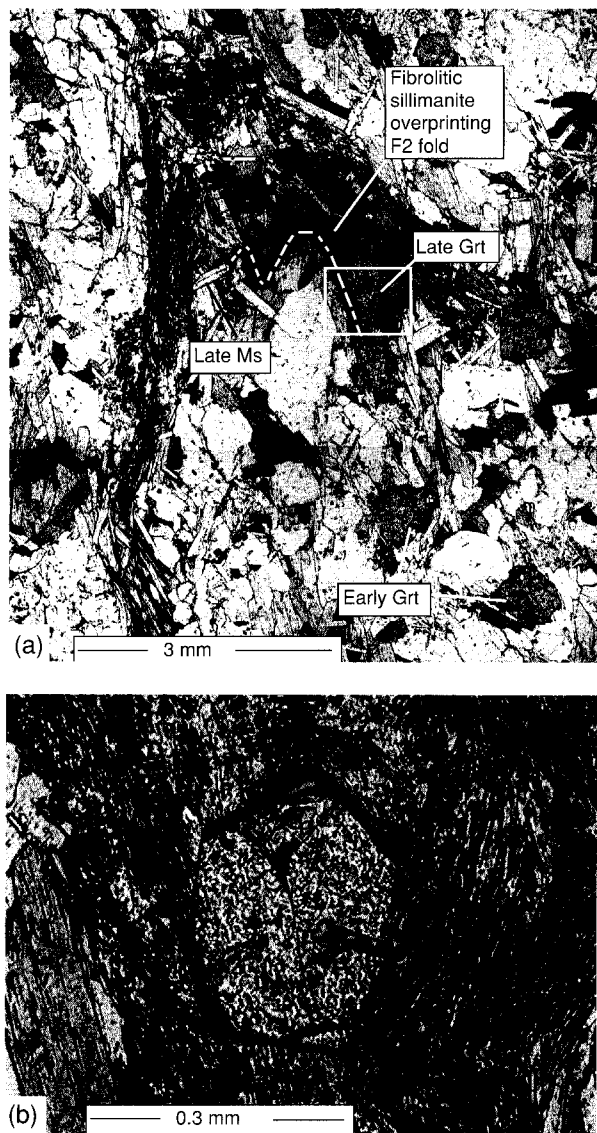
TABLE 1. Mineral assemblages of samples from the regional sillimanite zone

Sample	Qtz	Ms	Pl	Sil	Grt	Bt	Ilm	Gr	Po
BF-19	x	x	x	x	x	x	x	x	—
BF-78	x	x	x	x	x	x	x	—	—
89-1	x	x	x	x	x	x	x	—	—
89-6A	x	x	x	x	x	x	x	—	—
89-8B	x	x	x	x	x	x	x	x	x
89-9A	x	x	x	x	x	x	x	x	—
89-21A	x	x	x	x	x	x	x	x	—
89-22B	x	x	x	x	x	x	x	x	—
89-31A	x	x	x	x	x	x	x	x	—

Fig. 2. **(a)** Photomicrograph of a typical texture of the regional sillimanite zone (sample 89-1). Fibrolitic sillimanite replaces a small F_2 fold of muscovite. Two garnet crystals in the southeast quadrant are corroded (early garnet), whereas two smaller crystals within sillimanite are idioblastic (late garnet). Note the late muscovite cutting all fabrics. White box shows location of **b,** which is a detail of the idioblastic late garnet in a fibrolitic sillimanite clot.

developed and in many rocks forms the dominant fabric. A second schistosity (S_2) folds and crenulates S_1 and is locally penetrative. Kink banding is only observed locally. The origin of S_1 is unclear, but we interpret S_2 to correlate with regional recumbent fold formation ($=F_2$). Movement along the Fall Mountain and Chesham pond thrusts postdates recumbent fold formation but predates dome stage deformation. The dome stage folds trend northeast ($=F_3$) and east ($=F_4$), resulting in anticlinal and synclinal

culminations that expose, respectively, low and high structural levels but produced no obvious fabric.

Isograds shown in Figure 1 delineate the first appearance of the parageneses garnet, staurolite, sillimanite + muscovite, sillimanite + potassium feldspar and garnet + cordierite. There is a general trend toward increasing metamorphic grade from west to east. Significantly, the isograds in Figure 1 do not reflect the peak metamorphic mineral assemblage at any instant in time, but are the result of multiple generations of mineral growth. Examination of the cross section (Fig. 1b) reveals that the metamorphism in west-central New Hampshire is inverted, with the highest grade rocks occurring in the highest structural levels (Kruger, 1946; Chapman, 1953; Thompson et al., 1968; Spear et al., 1990b, 1993; Spear, 1992, 1993).

TEXTURES OF SILLIMANITE-BEARING ROCKS

Over 100 sample localities and over 300 samples from the study area (Fig. 1) have been examined petrographically. For this paper, 15 samples from the sillimanite zone have been examined in detail using X-ray compositional mapping and electron microprobe spot analyses.

Several textural varieties of sillimanite have been observed in the study area. The prominent textural types are indicated by the symbols in Figure 1, although many types can be found at any one locality. The most conspicuous are occurrences of prismatic sillimanite, interpreted to be pseudomorphs after andalusite (Fig. 1, squares), which occur in the Fall Mountain klippe (BF-9, BF-14) and in the root zone near Gilsum (BF-78) (See Fig. 2a of Spear et al., 1990a). Prismatic sillimanite also occurs within a muscovite pseudomorph that is interpreted as after andalusite (Fig. 1, inverted triangles) (BF-26). Fibrolitic sillimanite occurs locally inside muscovite (Fig. 1, triangles), both in the Fall Mountain klippe (BF-9, BF-14) (See Fig. 2d of Spear et al., 1990a) and in the Skitchewaug nappe (BF-86, BF-89, BF-92) (See Fig. 9d of Spear et al., 1990a). Fibrolitic sillimanite + biotite parageneses are restricted to the eastern part of the study area (Fig. 1, circles) (BF-19, BF-22, 89-1, 89-9, 89-6, 89-8, 89-21, 89-22, 89-31) and the Fall Mountain klippe (BF-9, BF-14). These occurrences will be referred to as the regional sillimanite zone.

Figure 2 shows a typical texture of the regional silli-

TABLE 2. Representative analyses of minerals from the regional sillimanite zone, west-central New Hampshire

	Representative garnet core analyses								
Sample	BF-19	BF-78	89-1	89-6A	89-8B	89-9A	89-21A	89-22B	89-31A
	Weight percent oxides								
SiO_2	36.82	38.35	37.35	37.28	36.96	37.51	37.51	36.70	37.51
Al_2O_3	21.70	20.99	21.48	21.12	20.95	21.29	21.93	21.56	22.39
MgO	2.86	2.77	2.76	2.82	2.66	3.02	3.61	2.34	3.55
FeO	27.82	29.93	31.49	30.87	31.83	28.22	25.16	36.10	26.06
MnO	9.80	7.07	7.04	7.26	7.27	8.91	11.32	3.34	9.98
CaO	1.61	1.04	1.17	1.15	0.91	1.36	2.00	1.27	2.94
Total	100.61	100.14	101.28	100.49	100.58	100.32	101.53	101.31	102.44
	Cations per 12 O atoms								
Si	2.953	3.066	2.981	2.996	2.983	3.005	2.962	2.947	2.936
Al	2.052	1.978	2.021	2.001	1.993	2.011	2.042	2.041	2.066
Mg	0.342	0.330	0.328	0.338	0.320	0.361	0.425	0.280	0.414
Fe^{2+}	1.866	2.001	2.102	2.075	2.148	1.891	1.662	2.424	1.706
Mn	0.666	0.479	0.476	0.494	0.497	0.605	0.757	0.227	0.662
Ca	0.138	0.089	0.100	0.099	0.079	0.117	0.169	0.109	0.247
Fe/(Fe + Mg)	0.845	0.858	0.865	0.860	0.870	0.840	0.796	0.896	0.805
Prp	0.114	0.114	0.109	0.112	0.105	0.121	0.141	0.092	0.137
Alm	0.620	0.690	0.699	0.690	0.706	0.636	0.552	0.797	0.563
Sps	0.221	0.165	0.158	0.164	0.163	0.203	0.251	0.075	0.219
Grs	0.046	0.031	0.033	0.033	0.026	0.039	0.056	0.036	0.082
	Plagioclase anorthite content								
Early	—	30	29	—	—	—	—	—	—
Peak	27	21	21	21	16	23	38	26	39
Late	—	—	—	—	—	—	28	—	—
	Representative analysis of biotite								
	Weight percent oxides								
SiO_2	35.28	35.11	35.35	35.32	35.73	35.75	37.04	34.85	37.11
Al_2O_3	19.14	18.60	19.10	19.26	19.20	19.43	19.03	19.39	19.23
TiO_2	2.10	2.90	2.23	1.95	2.32	2.02	1.83	2.41	2.88
MgO	10.34	8.96	9.15	9.12	9.11	10.08	12.48	7.90	11.82
FeO	17.05	18.92	20.22	19.93	20.67	18.70	15.28	22.24	15.93
MnO	0.16	0.05	0.08	0.09	0.08	0.08	0.24	0.02	0.26
CaO	0.15	0.06	0.02	0.02	0.04	0.04	0.05	0.01	0.01
Na_2O	0.18	0.21	0.29	0.26	0.29	0.15	0.21	0.27	0.18
K_2O	10.62	8.95	8.49	8.82	8.65	8.52	9.10	10.96	9.31
Total	95.01	93.75	94.93	94.77	96.08	94.76	95.24	98.04	96.72
	Cations per 11 O atoms (anhydrous)								
Si	2.685	2.707	2.697	2.700	2.698	2.707	2.751	2.638	2.724
[4]Al	1.315	1.293	1.303	1.300	1.302	1.293	1.249	1.362	1.276
[6]Al	0.402	0.398	0.415	0.436	0.407	0.442	0.417	0.368	0.388
Ti	0.120	0.168	0.128	0.112	0.132	0.115	0.102	0.137	0.159
Mg	1.173	1.030	1.041	1.039	1.025	1.138	1.381	0.891	1.293
Fe^{2+}	1.085	1.220	1.290	1.274	1.305	1.184	0.949	1.408	0.978
Mn	0.010	0.003	0.005	0.006	0.005	0.005	0.015	0.001	0.016
Σ oct	2.790	2.819	2.879	2.867	2.874	2.884	2.864	2.805	2.834
Ca	0.012	0.005	0.002	0.002	0.003	0.003	0.004	0.001	0.001
Na	0.026	0.031	0.043	0.038	0.042	0.022	0.030	0.039	0.026
K	1.031	0.880	0.826	0.860	0.833	0.823	0.862	1.058	0.872
Σ A	1.069	0.916	0.871	0.900	0.878	0.848	0.896	1.098	0.899
Fe/(Fe + Mg)	0.481	0.542	0.553	0.551	0.560	0.510	0.407	0.612	0.431
	Representative analyses of muscovite								
	Weight percent oxides								
SiO_2	45.90	45.08	45.76	46.19	46.86	46.72	48.79	45.89	
Al_2O_3	35.57	35.40	34.95	34.59	36.31	34.24	29.98	36.55	
TiO_2	0.68	0.69	0.63	0.75	0.67	0.83	0.38	0.77	
MgO	0.65	0.53	0.54	0.57	0.48	0.79	3.20	0.56	
FeO	1.04	1.06	0.87	0.84	1.02	1.03	2.09	1.15	
MnO	0.00	0.02	0.00	0.05	0.05	0.00	0.04	0.00	
CaO	0.06	0.00	0.01	0.03	0.01	0.00	0.00	0.03	
Na_2O	0.75	0.94	1.23	1.18	1.34	0.74	0.05	0.98	
K_2O	10.94	9.33	9.18	9.47	9.13	9.59	10.48	11.03	
Total	95.58	93.04	93.16	93.68	95.89	93.95	95.00	96.96	
	Cations per 11 O atoms (anhydrous)								
Si	3.052	3.054	3.090	3.108	3.074	3.131	3.264	3.014	
[4]Al	0.948	0.946	0.910	0.892	0.926	0.869	0.736	0.986	
[6]Al	1.841	1.881	1.872	1.852	1.882	1.836	1.628	1.844	

TABLE 2.—*Continued*

Sample	Representative analyses of muscovite								
	BF-19	BF-78	89-1	89-6A	89-8B	89-9A	89-21A	89-22B	89-31A
	Cations per 11 O atoms (anhydrous)								
Ti	0.034	0.035	0.032	0.038	0.033	0.042	0.019	0.038	
Mg	0.064	0.054	0.054	0.057	0.047	0.079	0.319	0.055	
Fe²⁺	0.058	0.060	0.049	0.047	0.056	0.058	0.117	0.063	
Mn	0.000	0.001	0.000	0.003	0.003	0.000	0.002	0.000	
Σ oct	1.997	2.031	2.007	1.997	2.021	2.015	2.085	2.000	
Ca	0.004	0.000	0.001	0.002	0.001	0.000	0.000	0.002	
Na	0.097	0.124	0.161	0.154	0.171	0.096	0.006	0.125	
K	0.928	0.806	0.791	0.813	0.764	0.820	0.894	0.924	
Σ A	1.029	0.930	0.953	0.969	0.936	0.916	0.900	1.051	
Fe/(Fe + Mg)	0.475	0.526	0.476	0.452	0.544	0.423	0.268	0.534	

Note: analytical procedures are identical to those described in Kohn et al. (1993).

manite zone. Fibrolitic sillimanite occurs in mats and as a replacement for muscovite and biotite. Locally, fibrolitic sillimanite is observed in folds, which are interpreted as F_2 nappe-related structures. The fibrolitic sillimanite is interpreted to have replaced folded muscovite, which places the fibrolitic sillimanite parageneses later than the D_2 deformation. Garnet in rocks of the regional sillimanite zone commonly show two textural habits. An early generation is typically 1–3 mm in diameter and displays evidence for resorption of the rim (early garnet in Fig. 2). In many localities, S_2 is flattened around early garnets, suggesting that early garnets grew prior to the development of S_2. A second generation is smaller (0.5–1 mm in diameter) and idioblastic and often occurs within clots of sillimanite, therefore postdating sillimanite growth (late garnet in Fig. 2a and detail in Fig. 2b). Muscovite also occurs in two habits: an early generation either lies within and helps to define the S_2 foliation or is folded by F_2 folds, and a later generation lies randomly across S_2.

MINERAL COMPOSITIONS AND ZONING

The typical, low-variance assemblage in schists of the regional sillimanite zone is garnet + biotite + (fibrolitic) sillimanite + muscovite + quartz + plagioclase. Mineral assemblages are listed in Table 1, and representative mineral analyses of assemblages that span the observed composition range are presented in Table 2. Garnet core compositions range from ~11 to 30 mol% spessartine + grossular, and there is a systematic partitioning of Fe, Mg and Mn + Ca between garnet and biotite (Fig. 3).

Chemical zoning in garnet is broadly symmetrical from core to rim (Figs. 4, 5), although early garnets (Fig. 4) may be nonconcentrically embayed by garnet-consuming reactions. Cores of early garnets are relatively homogeneous. Toward the rim of both early and late garnet, almandine, Fe/(Fe + Mg), and to a lesser degree grossular all increase, whereas spessartine and pyrope decrease. In samples that contain two generations of garnet, zoning in the outer rim is identical in both generations (compare Fig. 5a and 5b for sample 89-1).

Plagioclase is also zoned chemically with cores more calcic than rims. Moreover, inclusions of plagioclase within garnet are typically more calcic than matrix plagioclase. Porphyroblastic matrix biotite is generally homogeneous. Biotite inclusions within garnet invariably have a lower Fe/(Fe + Mg) than matrix biotite because inclusion biotite and host garnet have exchanged Fe and Mg during cooling. In one sample (BF-78), several inclusions of biotite within prismatic sillimanite have Fe/(Fe + Mg) that is higher than matrix biotite, although the Ti contents are identical.

THERMOBAROMETRY

P-T conditions calculated using garnet core compositions and matrix biotites, plagioclase, and muscovite are shown in Figure 6. The flat interiors of the garnets suggest that the core compositions of garnets larger than 1 mm have not been altered significantly since the metamorphic peak. Garnet + biotite Fe-Mg exchange thermometry (calibration of Hodges and Spear, 1982) yields temperatures that range from 575 to 625 °C at 3 kbar.

Plagioclase is zoned, and so it is a matter of interpretation as to which plagioclase compositions to use with garnet core compositions for geobarometry. Matrix plagioclase cores and plagioclase inclusions in garnet are more anorthitic and therefore yield lower pressures than do matrix plagioclase rims for a specific garnet composition. Garnet + plagioclase pressures calculated from the garnet + plagioclase + aluminum silicate + quartz (GASP) geo-
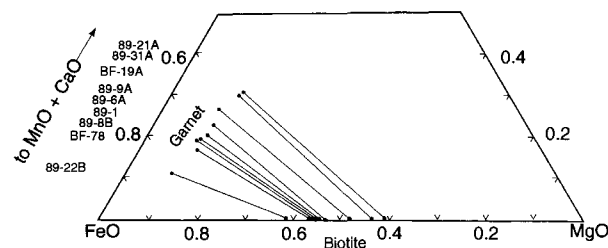

Fig. 3. Composition triangle (Fe, Mg, Mn + Ca) showing compositions of coexisting garnet + biotite from the regional sillimanite zone.
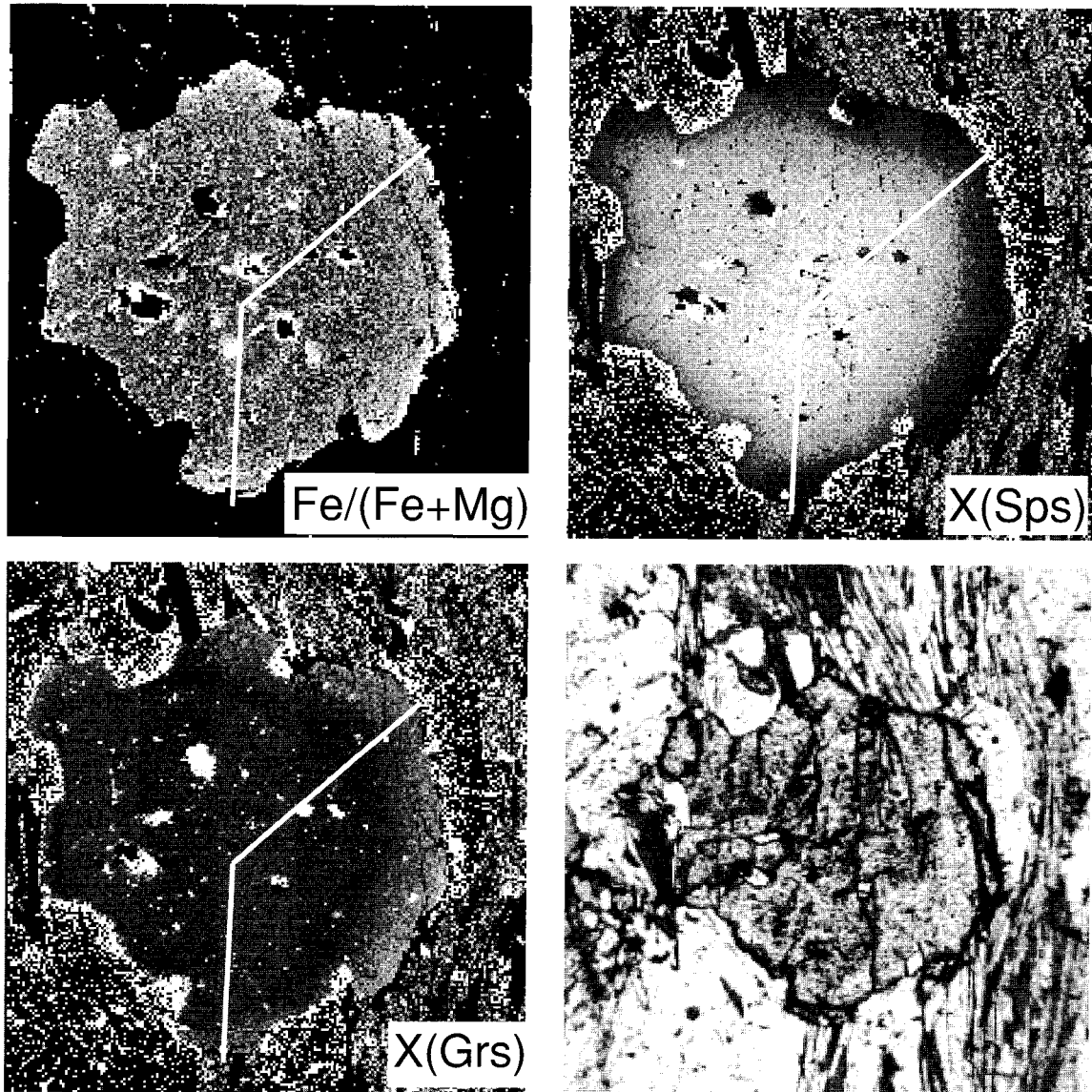
Fig. 4. X-ray composition maps and photomicrograph showing the zoning pattern of a typical garnet from the regional sillimanite zone. Light and dark areas are high and low and concentrations, respectively. This is an early garnet because it is corroded on the margins (especially on the left side), although the zoning on the rim is identical to the core-rim zoning of idioblastic garnets. Sample 89-22B. Width of image is 1.4 mm. White lines show position of traverse depicted in Fig. 5h.

barometer (calibration of Hodges and Spear, 1982) range from 2 to 5 kbar at 600 °C, and most samples cluster in the range of 3–4 kbar. Two samples (BF-78 and 89-1) have plagioclase with calcic cores that record pressures between 2 and 3 kbar at 600 °C, and one sample (89-21) has a late sodic plagioclase overgrowth that records a pressure of 5.1 kbar at 600 °C. Collectively, the garnet + plagioclase pressures imply an increase in pressure during garnet growth near the metamorphic peak or a decrease in temperature after the peak.

Pressures calculated using garnet + sillimanite + muscovite + biotite geobarometry (at 600 °C) yields pressures of 4.0–4.2 and 2.3–2.8 kbar using the calibrations of Hodges and Crowley (1985) and Holdaway et al. (1988), respectively. The consistency of pressures obtained from the Hodges and Crowley (1985) formulation with those from the Hodges and Spear (1982) GASP barometer is to be expected, inasmuch as Hodges and Crowley based their calibration on pressures determined from GASP.

PHASE EQUILIBRIA

One of the curious features of the paragenesis of the regional sillimanite zone rocks is that they do not appear to have ever contained staurolite, in spite of the abundance of staurolite in lower grade rocks. This seeming
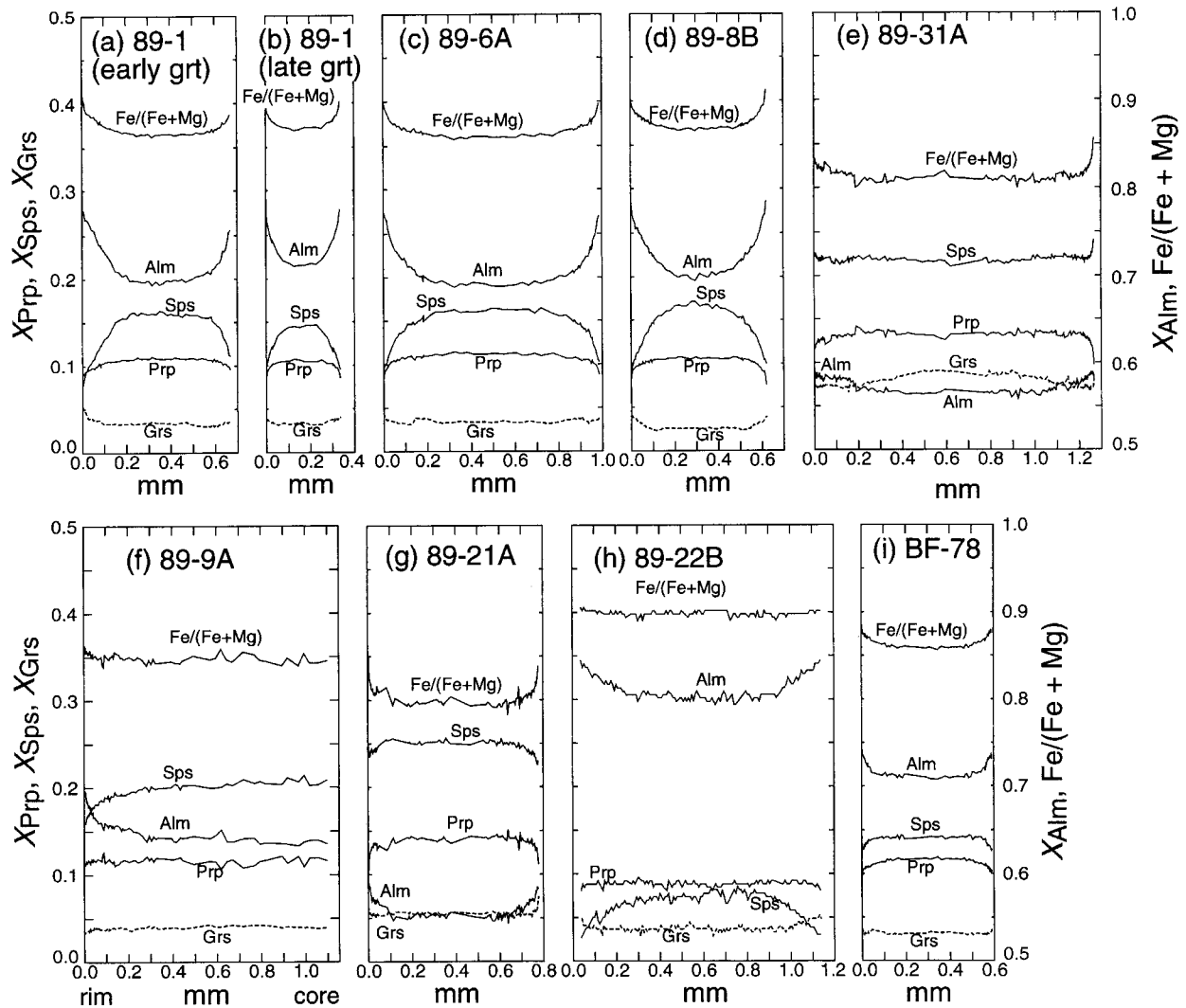
Fig. 5. Zoning profiles of garnets from nine samples (a–i) from the regional sillimanite zone. All traverses are rim to rim except for f (sample 89-9a), which is core to rim. Distance scale in each is identical. (h) Sample 89-22B is the same garnet featured in Fig. 4. Profiles in a and b are early (corroded) and late (idioblastic) crystals, respectively, from the same sample (89-1).

paradox can be explained by differences in bulk composition and the presence of extra components in garnet.

Figure 7 is a P-T diagram showing the invariant point garnet + biotite + chlorite + staurolite + Al_2SiO_5 (+ quartz + muscovite + H_2O) in the SiO_2-Al_2O_3-FeO-MgO-K_2O-H_2O (KFMASH) system. The absolute location of this invariant point is not known with certainty but may be inferred from differential thermodynamic analysis of assemblages following methods outlined by Spear and Cheney (1989). Moreover, extrapolation of the grid of Xu et al. (1994) indicates that this location is consistent with the data base of Holland and Powell (1990).

The reactions that emerge from the high-pressure side of this invariant point are garnet + chlorite = staurolite + biotite, staurolite + chlorite = Al_2SiO_5 (Ky, Sil, or And) + biotite, and staurolite = garnet + Al_2SiO_5 + biotite (Fig. 8). These three reactions have P-T slopes such

that they intersect again at ~15 kbar, forming a second occurrence of the same invariant point. The stable reactions that emanate to lower pressures are staurolite = garnet + chlorite + Al_2SiO_5 and garnet + chlorite = Al_2SiO_5 + biotite. It should be noted that both occurrences of the invariant point garnet + biotite + chlorite + staurolite + Al_2SiO_5 are probably metastable relative to chloritoid and cordierite-bearing assemblages, but the suite of rocks studied here do not contain either of these phases because their Fe/Mg is too low for chloritoid and too high for cordierite.

As shown by the large arrow in Figure 8, along P-T paths at pressures below the low pressure occurrence of the garnet + biotite + chlorite + staurolite + Al_2SiO_5 invariant point, garnet + chlorite + biotite assemblages react directly to produce aluminum silicate assemblages with no intervening staurolite. At pressures above the
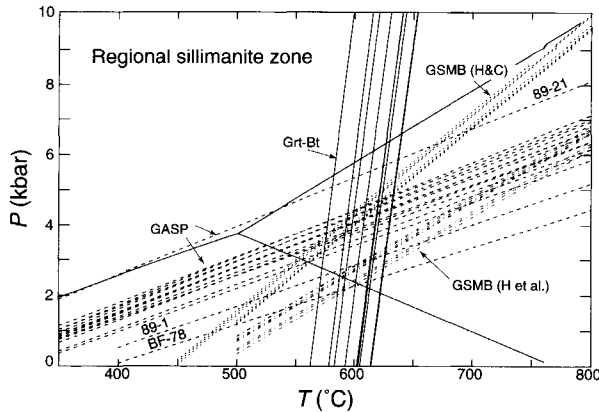
Fig. 6. *P-T* diagram showing temperatures and pressures calculated from different thermobarometers for the regional sillimanite zone. Solid lines (Grt-Bt) are the garnet + biotite Fe-Mg exchange thermometer (calibration of Hodges and Spear, 1982); dashed lines (GASP) are garnet + plagioclase + sillimanite + quartz barometer (calibration of Hodges and Spear, 1982); dotted lines (GSMB: H&C) are garnet + sillimanite + muscovite + biotite barometer (calibration of Hodges and Crowley, 1985). Dot-dashed lines (GSMB: H et al.) are garnet + sillimanite + muscovite + biotite barometer (calibration of Holdaway et al., 1988). *P-T* conditions at the peak temperature are inferred to be 600–625 °C, 3.5–4.2 kbar.

invariant point, garnet + biotite + chlorite assemblages first form staurolite, which reacts to form aluminum silicate.

With the addition of MnO and CaO to the system, the stability of garnet-bearing assemblages increases because garnet incorporates these components preferentially to other minerals in this system. To a first order, the effect is to move the two KFMASH invariant points (garnet + biotite + chlorite + staurolite + Al_2SiO_5) closer together along the garnet-absent reaction staurolite + chlorite = aluminum silicate + biotite. Figure 7 also shows the effect of adding MnO to the system calculated using differential thermodynamics (the Gibbs method: Spear, 1988a). In this application, Mn was added to garnet, biotite, and staurolite in proportions consistent with observed partitioning. The results are contoured as a spessartine component in garnet. The field for staurolite collapses with increasing MnO and completely disappears at the point where garnet composition is $X_{Sps} \approx 0.3$.

In order to compare the theoretical analysis of Figure 7 with the compositions of the samples, it is necessary to project the compositions of the minerals into the CaO-free system. Spear (1988b) described a scheme of "ther-

modynamic projection," in which the compositions of minerals may be adjusted to any bulk composition, subject to the constraints imposed by the thermodynamic equilibrium constants. For the present study, mineral compositions were projected to values of $X_{Grs} \approx 0$. Note that this procedure does not give the same result as simply renormalizing without Ca.

The results for the sillimanite zone samples are plotted in Figure 9a. The partitioning systematics are similar to those shown in Figure 3, except that garnet and biotite both plot closer to the FeO apex and both have higher Fe/(Fe+ Mg). Samples 89-22B has the lowest MnO content, with $X_{Sps} = 0.072$. For comparison, the same plot for samples from the staurolite zone is shown in Figure 9b. Staurolite parageneses are restricted to low values of X_{Sps} in garnet, and the maximum recorded value for a staurolite-bearing sample is $X_{Sps} = 0.082$ (sample BF-38B). Sample BF-26A is noteworthy because it contains sillimanite + biotite, but it is from a locality where staurolite is common. As can be seen, this sample has $X_{Sps} = 0.11$, which is too high for the production of staurolite.

The minimum X_{Sps} found in rocks that display the reaction garnet + chlorite = aluminum silicate + biotite (i.e., no staurolite parageneses) provides bounds on the pressure of the *P-T* path. Inasmuch as andalusite is observed locally, the lower pressure occurrence of the garnet + biotite + chlorite + staurolite + Al_2SiO_5 invariant point is the appropriate one for these samples, and from it an upper boundary on the pressure of the *P-T* path can be obtained. The Mn-absent (KFMASH) invariant point is located at ≈ 1.5 kbar, and an increase in X_{Sps} of 0.072 (the minimum projected composition of garnet in staurolite-absent rocks) moves the invariant point to ~ 2.5 kbar. This means the *P-T* path must have passed below ≈ 2.5 kbar at ≈ 560 °C. This pressure limit, of course, depends critically on the placement of the KFMASH invariant point (garnet + biotite + chlorite + staurolite + Al_2SiO_5). If the invariant point is moved to lower or higher pressure, the maximum pressure boundary moves to lower or higher pressure, respectively.

The *P-T* path shown in Figure 7 produces andalusite, not sillimanite, when the reaction garnet + chlorite = aluminosilicate + biotite is encountered. Within uncertainty, this problem could be avoided by moving the invariant point to higher pressure. For example, a shift of the KFMASH invariant point from 1.5 to 2.5 kbar would place a maximum pressure of ≈ 3.5 kbar on the *P-T* path, and the reaction garnet + chlorite = aluminosilicate + biotite would proceed in the sillimanite field. However, it is also possible that fibrolitic sillimanite was produced

$\rightarrow$

Fig. 7. *P-T* diagram showing the effect of the addition of MnO to the KFMASH invariant point garnet + biotite + chlorite + staurolite + Al_2SiO_5. Dotted lines are KFASH reactions, solid lines are KFMASH reactions, and dashed lines are the reactions garnet + chlorite = staurolite + biotite and staurolite = garnet + Al_2SiO_5 + biotite at values of $X_{Sps} = 0.1$ and 0.2. Note that, as X_{Sps} in garnet increases, the stability field for the reaction garnet + chlorite = Al_2SiO_5 + biotite increases. Thick, gray line is the inferred *P-T* path.
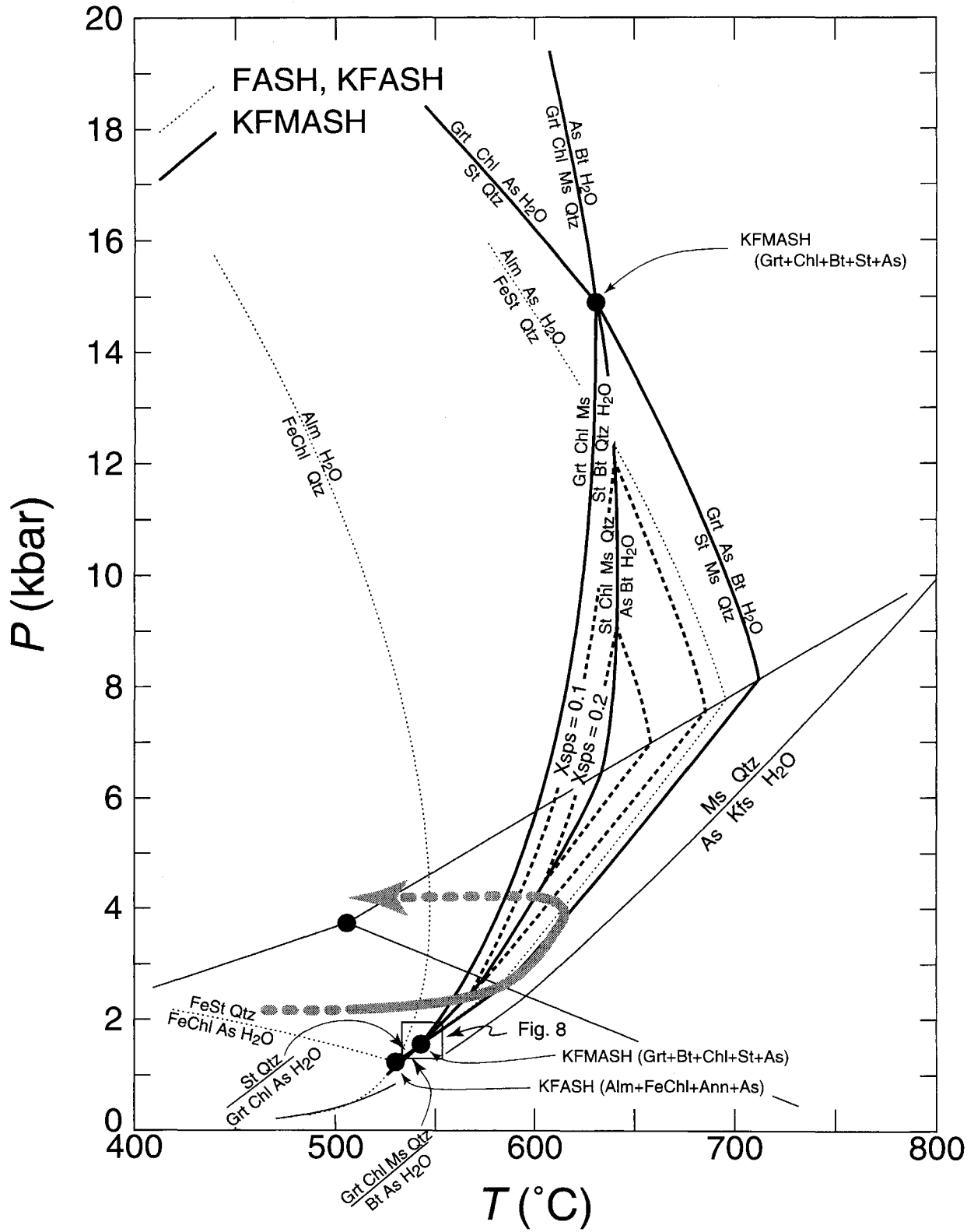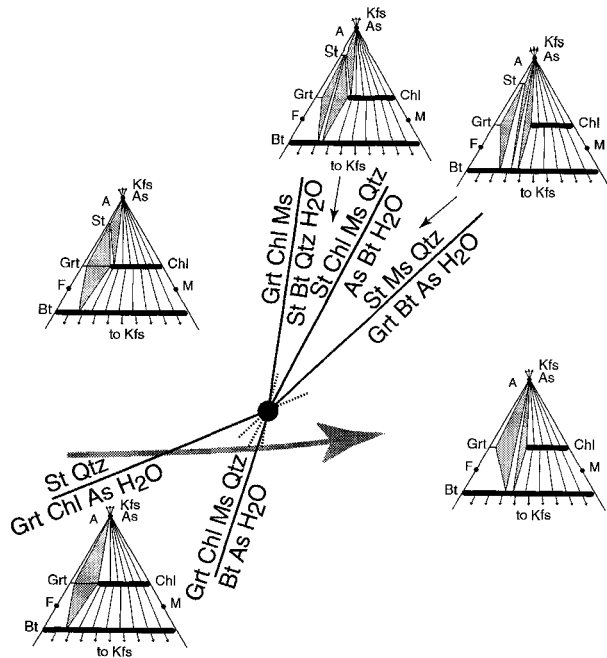
Fig. 8. Schematic representation of the KFMASH invariant point garnet + biotite + chlorite + staurolite + Al₂SiO₅ showing P-T paths (gray arrow) along which the low-grade assemblage garnet + chlorite (in Al-poor rocks) reacts directly to form Al₂SiO₅ + biotite with no intervening staurolite.
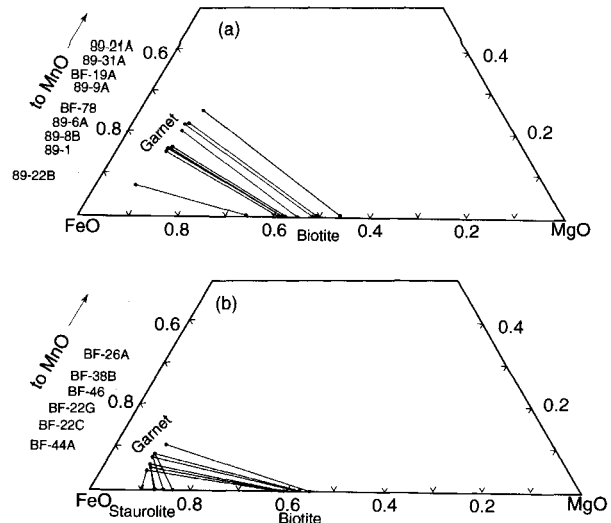

Fig. 9. Composition triangles (Fe, Mg, Mn) showing projected compositions of coexisting garnet + biotite. (a) Regional sillimanite zone. (b) Staurolite zone. The compositions of garnet and biotite have been projected to $X_{Grs} = 0.0001$ following the method of Spear (1988b).

metastably relative to andalusite (or prismatic sillimanite). Therefore, the production of fibrolitic sillimanite rather than andalusite can also be used to constrain the pressure of the P-T path.

PTXM PHASE EQUILIBRIA

Analysis of the PTXM (pressure-temperature-composition-mode) phase relations of the assemblage garnet + biotite + sillimanite + muscovite + quartz provides additional constraints on the P-T path followed by samples from the regional sillimanite zone. Four observations are relevant: (1) the growth of secondary garnet, (2) the chemical zoning observed on the rims of garnet, and (3) the composition shift between biotite inclusions within sillimanite (after andalusite) porphyroblasts and matrix biotite, and (4) the composition shift in plagioclase between plagioclase core and rim and between plagioclase inclusions within garnet and matrix plagioclase.

Following methods described by Spear (1988a, 1989), P-T diagrams contoured for mineral compositions and abundance have been constructed. The necessary input

data include the entropies and volumes of all phases as a function of pressure, temperature, and composition, and an equilibrated reference assemblage of known PTXM. The diagram in Figure 10 has been constructed using sample 89-1 (Table 3) as a reference assemblage at 620 °C, 4 kbar, and the thermodynamic data listed in Spear and Cheney (1989; after Berman, 1988).

The P-T trajectory shown in Figure 10a–10h is based on the zoning observed in the two garnet generations (Figs. 4, 5). The ratio Fe/(Fe + Mg) increases, whereas X_{Sps} decreases, and the only path that is consistent with these changes is one of nearly isobaric cooling (Fig. 10c, 10e). Indeed, the path is fairly tightly constrained because the Fe/(Fe + Mg) and X_{Sps} isopleths intersect at a fairly low angle and the path is constrained to pass through the acute angle of this intersection. It should be noted, however, that the isopleths shown in Figure 10 are based on the assumption of a closed system with a constant bulk composition in which all phases are at all times homogeneous, which is not valid in the case where diffusive fluxes across the garnet rim occur nor where garnet fractionally crystallizes. Modification to the path based on a diffusion analysis will be presented below.

Biotite Fe/(Fe + Mg) isopleths help constrain the early P-T path. A biotite inclusion within porphyroblastic sillimanite (after andalusite) from sample BF-78 has an Fe/

→

Fig. 10. P-T diagrams showing isopleths of garnet composition (a)–(e), garnet molar abundance (f), plagioclase composition (g), biotite composition (h). P-T path shows the inferred trajectory that results in the chemical zoning on the rims of garnet. Shaded isopleth in g shows the composition of early plagioclase inclusions in garnet. Shaded box in h shows the part of the biotite isopleth that corresponds to the composition of biotite inclusions in andalusite.
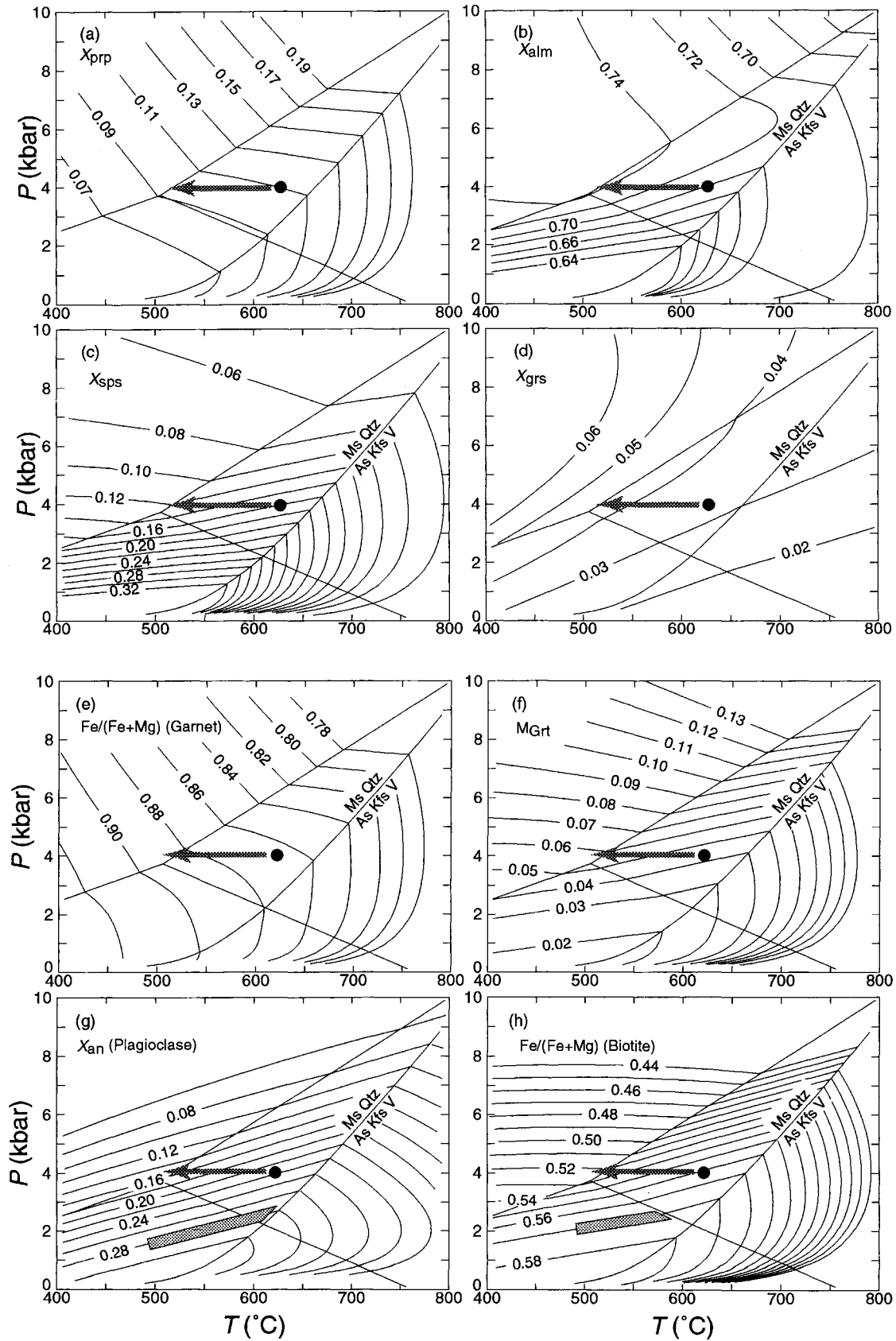
TABLE 3. Mineral abundance and compositions used as reference for calculation of PTXM phase diagram (Fig. 10) and diffusion model (Fig. 11)

Mineral	V of phase (%)	Molar proportion of phase	Component	Mole fraction	Activity model (a)
Quartz (Qtz)	30	0.688	quartz (Qtz)	1.0	1
H_2O (V)	0	0	H_2O	1.0	1
Sillimanite (Sil)	5	0.054	sillimanite (Sil)	1.0	1
Muscovite (Ms)	20	0.076	muscovite (Ms)	1.0	1
Garnet (Grt)	5	0.023	pyrope (Prp)	0.109	$(X_{Prp})^3$
			almandine (Alm)	0.699	$(X_{Alm})^3$
			spessartine (Sps)	0.158	$(X_{Sps})^3$
			grossular (Grs)	0.033	$(X_{Grs})^3$
Biotite (Bt)	30	0.105	phlogopite (Phl)	0.445	$(X_{Phl})^3$
			annite (Ann)	0.552	$(X_{Ann})^3$
			manganese biotite (MnBt)	0.002	$(X_{MnBt})^3$
Plagioclase (Pl)	10	0.054	albite (Ab)	0.78	X_{Ab}
			anorthite (An)	0.22	X_{An}

Note: $T = 625\ °C$; $P = 4000$ bars. System components = SiO_2, Al_2O_3, MgO, FeO, MnO, CaO, Na_2O, K_2O, H_2O.

(Fe + Mg) of 0.572, compared with the composition of 0.552 for the biotite in the matrix. Assuming that the biotite inclusion equilibrated with the assemblage garnet + biotite + aluminum silicate and that it preserved its composition since entrapment, the P-T path is then constrained to cross the Fe/(Fe + Mg) = 0.572 isopleth in the andalusite field (shaded area in Fig. 10h).

A similar constraint is obtained from consideration of plagioclase inclusions within garnet and zoning in matrix plagioclase. Plagioclase cores and inclusions within garnet are always more calcic than the rims of matrix plagioclase. For example, plagioclase in sample 89-1 is zoned from An_{28} to An_{22}. It is not known at what point the core of the plagioclase grew, but it is clear from Figure 10g that these early plagioclase compositions signify a lower pressure than the metamorphic peak.

DIFFUSION MODELING

Spear (1991), Spear and Florence (1992), and Florence and Spear (1993) modeled the evolution of garnet zoning profiles by incorporating both phase equilibria and diffusion kinetics. Their finite difference procedure involves (1) incrementing temperature and pressure along a presumed P-T path, (2) calculation of the equilibrium composition of the rim of the garnet at the new P-T conditions, (3) calculating the effects of diffusion in garnet by prescribing a time step, (4) computing the mass flux across the garnet rim and incorporating this flux into the matrix as a bulk composition shift. The procedure is then repeated over the length of the P-T path. This procedure more accurately reflects actual processes that occur in a rock during the evolution of a garnet zoning profile than the simple inferences drawn from PTXM phase diagrams (e.g., Fig. 10). Moreover, it is possible to compare the particular shape of the zoning profile with that predicted by the model and to place constraints on the rate of heating or cooling.

Samples 89-1 was chosen for this analysis because the sample history is well characterized and there are two generations of garnet to compare against model results

(Figs. 2, 5). A nearly isobaric cooling path is required to generate the observed core to rim variations in garnet composition (Fig. 10), but it is not apparent from examination of the zoning profiles in the two generations of garnet whether the shape of the zoning profile is due to fractionation during growth or diffusion. It is clear, however, that volume diffusion driven by simple exchange at the garnet rim on cooling cannot produce the observed zoning because exchange reactions are incapable of producing the downward trend in spessartine or the small increase in X_{Grs}.

Model garnet zoning profiles are superimposed on the measured profiles for two garnets from sample 89-1 (Fig. 11). In all models, an attempt was made to match the spessartine zoning profile as closely as possible, and so the match in spessartine is optimal. Comparisons using other elements are then measures of how well the overall model explains the observed profile. Diffusion coefficients of Loomis et al. (1985) were used, which, at 600 °C, are ~1.5 orders of magnitude larger than those of Chakraborty and Ganguly (1992). The effect of slower diffusion would be to decrease model values of cooling rates by 1-2 orders of magnitude, as discussed below.

Figure 11a shows several models that examine the importance of diffusion in generating the zoning observed in the primary garnet (cf. Fig. 5a). A homogeneous garnet with an intial radius of 300 μm was assumed, and a minimal amount of growth on the rim of the garnet was employed as a mechanism to change the boundary condition. Calculations were made assuming cooling rates of infinite, 100, 10, and 1 °C/m.y. There is a poor match between the observed and calculated profiles, irrespective of the cooling rate, and the match is poorest on the left side of the crystal. Indeed, the mere existence of an asymmetric zoning profile suggests that diffusion is not the sole mechanism by which garnet has changed its composition, inasmuch as diffusion is most likely to act symmetrically on a crystal, provided all surfaces of the crystal maintain the same boundary composition, which appears to be the case here. The reason for the poor match is that rapid cooling rates only allow diffusion to affect the near rim
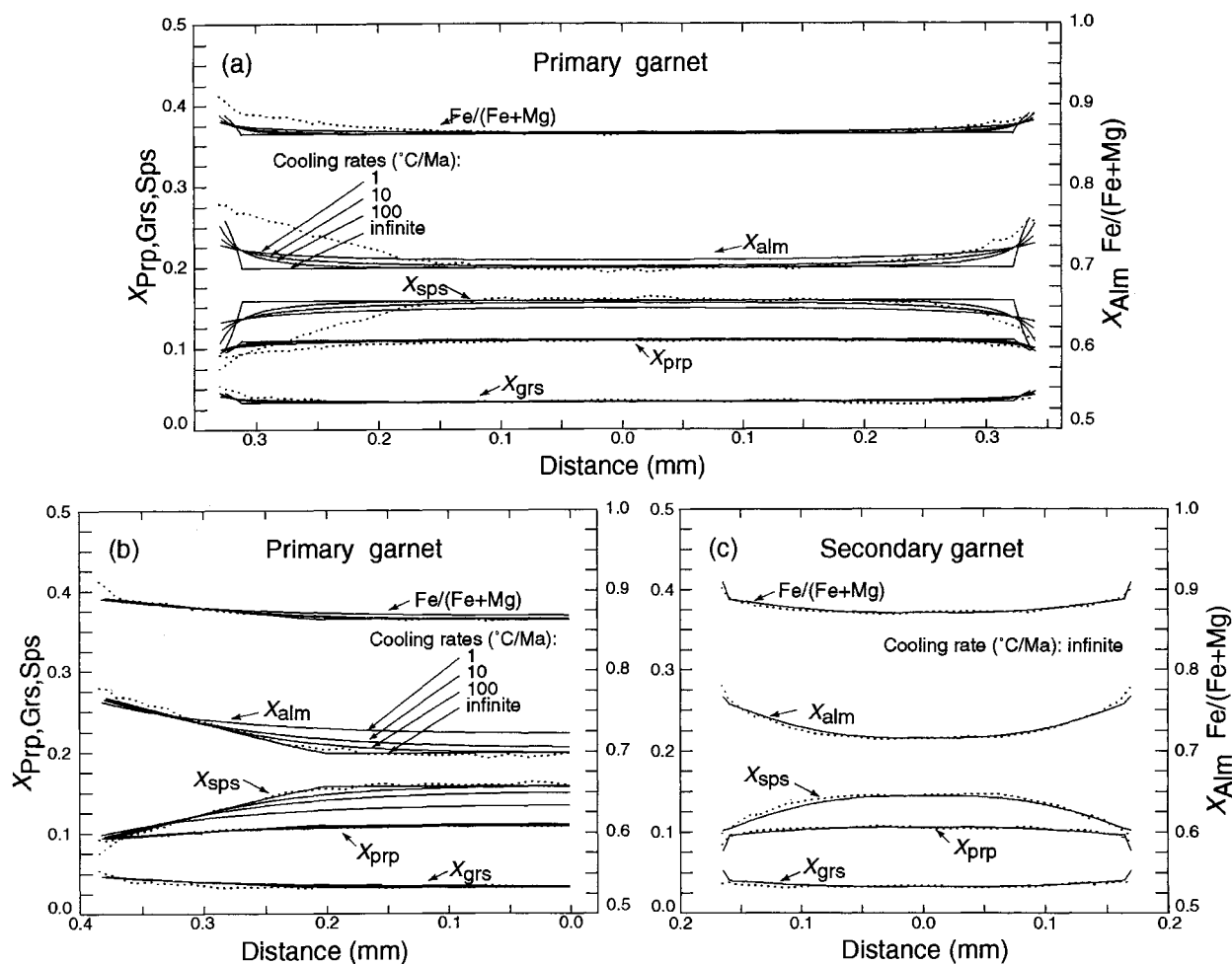
Fig. 11. Composition vs. distance profiles for model (solid lines) and observed (dotted lines: sample 89-1) garnet zoning. (a) Models dominated by diffusion (only very minor growth). Cooling rates are infinite, 100, 10, and 1 °C/m.y. (b) Models that incorporate growth of ~170 μm on the rim of a preexisting garnet with a 200-μm radius. Cooling rates are infinite, 100, 10, and 1 °C/m.y. (c) Model of secondary garnet zoning (sample 89-1) in which continuous reactions operate down to 525 °C and Fe-Mg exchange reactions only operate below 525 °C. Cooling rate is infinite.

of the garnet, whereas slow cooling allows diffusion to affect the core.

Figure 11b shows a model designed to match to the left side of the primary garnet (Fig. 5a), if one assumes growth is the principal mechanism. A homogeneous garnet with an initial radius of 200 μm was assumed, which corresponds to the radius at the break in composition slope. Growth of ~170 μm of garnet was permitted over a temperature interval of 625–450 °C. Four models were generated, corresponding to cooling rates of infinite, 100, 10, and 1 °C/m.y. The model that best appears to fit the observed zoning is the one that assumes infinite cooling rate (i.e., growth only). Diffusion, even at 100 °C/m.y. has the effect of flattening the profile more than is observed.

To test further the hypothesis that the zoning is dominantly growth zoning, two models were used to match

the zoning observed in the secondary garnet (Fig. 11c). In these models, the starting conditions assumed no initial garnet present and the cooling rate was again assumed to be infinite. In the first model was assumed continuous reaction from the starting conditions of 620 °C, 4 kbar, down to 450 °C. This model fits the zoning profile quite well in the garnet interior, and the rim spessartine and grossular compositions match quite well. However, the values for the model Fe/(Fe + Mg) and almandine are a bit too low and the pyrope values too high, compared with the measured profile. In the second model, continuous reactions were allowed to operate from 620 to 525 °C, and then only Fe-Mg exchange between garnet and biotite was allowed to occur during the last increment of decreasing temperature, which affects almandine and pyrope, but not spessartine. The model matches the observed outer rim composition quite closely (Fig. 11c).

From these models we conclude that there is very little diffusional zoning in garnets from the area; virtually all the zoning appears to be the result of growth on cooling. This then implies that postpeak metamorphic cooling was quite rapid down to the closure temperature of garnet-biotite Fe-Mg exchange (~500 °C). This, however, does not rule out the possibility that diffusional processes homogenized the garnets at conditions near the metamorphic peak, as suggested earlier, implying an extended period of time at the peak conditions.

COMPARISON WITH PREVIOUS WORK AND TECTONIC IMPLICATIONS

The parageneses of rocks examined in this study can be explained by a counterclockwise P-T path that involves a period of isobaric heating followed by loading. We suggest that this path is the result of loading beneath a thrust nappe, in which case the ~2-kbar increase implies ~7 km of crustal thickening. The Chesham Pond thrust (Fig. 1) lies to the east, structurally above the regional sillimanite zone, and is a possible candidate. This interpretation requires movement along the Chesham Pond thrust after the development of the nappe stage fabrics, consistent with the interpretation of Thompson (1985, 1988), Robinson et al. (1991), Kohn et al. (1992), and Florence et al. (1993). An alternative hypothesis is that the increase in pressure arose from the intrusion of high-level plutons (now eroded). Guidotti and Holdaway (1993) have described post-tectonic, regional contact metamorphism in northwestern Maine, which is associated with plutons with ages ranging from 399 to 325 m.y. If similar plutons intruded in the vicinity of the study area, that might provide the necessary increase in crustal thickness.

Chamberlain (1986) presented an alternative interpretation of the metamorphism of this area as having resulted from the folding of thermal surfaces during postnappe F_3 and F_4 folding. (In Chamberlain's work, dome stage folds are designated F_2 and east-trending open folds are designated F_3.) In his view, F_3 and F_4 anticline intersections (A_3A_4) experienced postnappe cooling during recrystallization, whereas rocks from intersections of F_3 and F_4 synclines (S_3S_4 intersections) experienced postnappe heating and burial. This heating and cooling resulted in localized, highly variable P-T paths that he used to explain locally variable garnet, sillimanite, and biotite parageneses.

We did not find the same systematic variation in mineral parageneses reported by Chamberlain (1986). Conversely, we found that resorption textures of garnet are ubiquitous over the regional sillimanite zone and are independent of location in postnappe-stage anticlines or synclines. Moreover, we interpret the two generations of garnet within individual samples as having arisen from Reaction 1 and a single counterclockwise P-T loop. Chamberlain (1986) did not report two generations of garnet from individual samples and consequently postu-lated diverse P-T paths for samples with resorbed vs. idioblastic garnet.

Not every rock contains small, idioblastic garnets as evidence for late garnet growth during cooling. Such an absence in some rocks may readily be explained in one of two ways. (1) A slight decrease in pressure during cooling results in the P-T path following a garnet molar isopleth, along which garnet is neither produced nor consumed (Fig. 10f). If there were small changes in erosional level during cooling, then rocks in one part of the area would grow garnet, whereas rocks in other parts would not. (2) Secondary garnets are only produced if conditions are appropriate for nucleation. Late growth of garnet on preexisting garnet is harder to identify petrographically than new growth of idioblastic garnets. For example, our interpretation of late garnet overgrowths is based on extensive X-ray mapping to determine garnet zoning and diffusion analysis to rule out the possibility that the rims were produced by diffusion and not growth.

Two other lines of evidence suggest that metamorphic recrystallization in the regional sillimanite zone is not in response to the folding of isotherms. (1) Examination of Figure 1a reveals that sample 89-22 is from a high-amplitude, dome-stage syncline between the Alstead and Keene domes, and yet it displays an identical paragenesis to A_3A_4 sample 89-1. (2) Preliminary work on S_3S_4 samples (e.g, sample LM-1, Fig. 1; Spear et al., 1990b; Spear, 1992) indicates a simple P-T history involving early heating at low pressure followed by nearly isobaric cooling; we have found no evidence for an increase in pressure from 5 to 6 kbar and a simultaneous increase in temperature, as reported by Chamberlain (1986). Indeed, the simplest interpretation is that the metamorphic sequence in the region is inverted, with the highest grade rocks in the structurally highest positions, similar to the well documented metamorphism at Fall Mountain to the west (Thompson et al., 1968; Spear et al., 1990a). Late folding depressed high-grade rocks to the same physical level as lower grade rocks, yielding the isograd pattern of Figure 1a following erosion.

Cooling rates calculated from the present study (>100 °C/m.y.) are similar to those calculated by Muncill and Chamberlain (1988) (55–120 °C/m.y.). Both studies used the relatively rapid diffusion coefficients of Loomis et al. (1985) and Cygan and Lasaga (1985), respectively; with the diffusion coefficients of Chakraborty and Ganguly (1992), the inferred cooling rates are 1–2 orders of magnitude slower (i.e., 1–10 °C/m.y.). Uncertainty in the rate of volume diffusion in garnet propagates to a large uncertainty in calculated cooling rates and, consequently, significant differences in the implied rate of tectonic transport and exhumation. The rapid cooling inferred from the diffusion analysis using the coefficients of Loomis et al. (1985) or Cygan and Lasaga (1985) requires either tectonic denudation, extremely rapid uplift, and erosion or tectonic transport onto cool basement rocks, whereas the slower cooling inferred from the diffusion analysis

using the coefficients of Chakraborty and Ganguly (1992) may be achieved by less extreme processes. Unfortunately, geochronology does not sufficiently constrain the cooling rate to permit a distinction to be made between these options. U-Pb dates on monazite ($T_c \approx 700$ °C: Heaman and Parrish, 1991) indicate the peak of metamorphism is at $\sim$390–400 Ma (Eusden and Barreiro, 1988), whereas the oldest hornblende $^{40}Ar/^{39}Ar$ cooling ages are $\sim$350 Ma (Harrison et al., 1989). The temperature difference between the metamorphic peak and hornblende closure is $\sim$125 °C, indicating an average cooling rate of 125 °C/ 50 m.y. = 2–3 °C/m.y. However, it is equally possible that the cooling rate was considerably more rapid near the metamorphic peak (ca. 100 °C/m.y.), and then slowed considerably after the rocks fell below 550 °C.

The interpretation that relatively high bulk MnO contents are responsible for the paragenesis garnet + chlorite = sillimanite + biotite has implications for the stratigraphic correlations implicit in Figure 1. Rocks that are high in MnO have been mapped as the Partridge, Rangeley, and Littleton Formations, whereas rocks that are low in MnO (staurolite-bearing) have been mapped as both Partridge and Littleton. If stratigraphy correlates with bulk composition, then clearly a revision of the map stratigraphic assignments in Figure 1 is required. We suggest that most of the metapelitic schists east of the regional sillimanite isograd are in fact Rangeley.

ACKNOWLEDGMENTS

REFERENCES CITED

Allen, T. (1984) The Fall Mountain outlier: A piece of the Fall Mountain nappe. B.A. honors thesis, Harvard University, Cambridge, Massachusetts.

Berman, R.G. (1988) Internally-consistent thermodynamic data for minerals in the system $Na_2O-K_2O-CaO-MgO-FeO-Fe_2O_3-Al_2O_3-SiO_2-TiO_2-H_2O-CO_2$. Journal of Petrology, 29, 445–522.

Chakraborty, S., and Ganguly, J. (1992) Cation diffusion in aluminosilicate garnets: Experimental determination in spessartine-almandine diffusion couples, evaluation of effective binary diffusion coefficients, and applications. Contributions to Mineralogy and Petrology, 111, 74–86.

Chamberlain, C.P. (1985) Tectonic and metamorphic history of a high-grade terrane, southwestern New Hampshire. Ph.D. dissertation, Harvard University, Cambridge, Massachusetts.

——— (1986) Evidence for the repeated folding of isotherms during regional metamorphism. Journal of Petrology, 27, 63–89.

Chapman, C.A. (1953) Problem of inverted zones of metamorphism in western New Hampshire. Illinois State Academy of Sciences Transactions, 46, 115–123.

Cygan, R.T., and Lasaga, A.C. (1985) Self-diffusion of magnesium in garnet at 750 ° to 900 °C. American Journal of Science, 285, 328–350.

Eusden, J.D., and Barreiro, B. (1988) The timing of peak high-grade metamorphism in central-eastern New England. Maritime Sediments and Atlantic Geology, 24, 241–255.

Florence, F.P., and Spear, F.S. (1993) Influences of reaction history and chemical diffusion on $P-T$ calculations for staurolite schists from the Littleton Formation, northwestern New Hampshire. American Mineralogist, 78, 345–359.

Florence, F.P., Spear, F.S., and Kohn, M.J. (1993) $P-T$ paths from northwestern New Hampshire: Metamorphic evidence for stacking in a thrust/ nappe complex. American Journal of Science, 293, 939–979.

Guidotti, C.V., and Holdaway, M.J. (1993) Petrology and field relations of successive metamorphic events in pelites of west-central Maine. Field Trip Guidebook for the Northeastern United States: Annual Meeting of the Geological Society of America, Boston, Massachusetts, 1, L1–L26.

Harrison, T.M., Spear, F.S., and Heizler, M. (1989) Geochronologic studies in central New England: II. Post-Acadian hinged and differential uplift. Geology, 17, 185–189.

Heaman, L., and Parrish, R. (1991) U-Pb geochronology of accessory minerals. In L. Heaman and J.N. Ludden, Eds., Applications of radiogenic isotope systems to problems in geology. Mineralogical Association of Canada Shortcourse Handbook, 19, 59–102.

Hodges, K.V., and Crowley, P.D. (1985) Error estimation and empirical geothermobarometry for pelitic systems. American Mineralogist, 70, 702–709.

Hodges, K.V., and Spear, F.S. (1982) Geothermometry, geobarometry and the Al_2SiO_5 triple point at Mt. Moosilauke, New Hampshire. American Mineralogist, 67, 1118–1134.

Holdaway, M.J., Dutrow, B.L., and Hinton, R.W. (1988) Devonian and Carboniferous metamorphism in west-central Maine: The muscovite-almandine geobarometer and the staurolite problem revisited. American Mineralogist, 73, 20–47.

Holland, T.J.B., and Powell, R. (1990) An enlarged and updated internally consistent thermodynamic dataset with uncertainties and correlations: The system $K_2O-Na_2O-CaO-MgO-MnO-FeO-Fe_2O_3-Al_2O_3-TiO_2-SiO_2-C-H_2-O_2$. Journal of Metamorphic Geology, 8, 89–124.

Kohn, M.J., Orange, D.L., Spear, F.S., Rumble, D., III, and Harrison, T.M. (1992) Pressure, temperature, and structural evolution of west-central New Hampshire: Hot thrusts over cold basement. Journal of Petrology, 33, 521–556.

Kohn, M.J., Spear, F.S., and Dalziel, I.W.D. (1993) Metamorphic $P-T$ paths from Cordillera Darwin, a core complex in Tierra del Fuego, Chile. Journal of Petrology, 34, 519–542.

Kruger, F.C. (1946) Structure and metamorphism of the Bellows Falls Quadrangle of New Hampshire and Vermont. Geological Society of America Bulletin, 57, 161–206.

Loomis, T.P., Ganguly, J., and Elphick, S.C. (1985) Experimental determinations of cation diffusivities in aluminosilicate garnets: II. Multicomponent simulation and tracer diffusion coefficients. Contributions to Mineralogy and Petrology, 90, 45–51.

Muncill, G.E., and Chamberlain, C.P. (1988) Crustal cooling rates inferred from homogenization of metamorphic garnets. Earth and Planetary Science Letters, 87, 390–396.

Robinson, P., Thompson, P.J., and Elbert, D.C. (1991) The nappe theory in the Connecticut Valley region: Thirty-five years since Jim Thompson's first proposal. American Mineralogist, 76, 689–712.

Spear, F.S. (1988a) The Gibbs method and Duhem's theorem: The quantitative relationships among P, T, chemical potential, phase composition and reaction progress in igneous and metamorphic systems. Contributions to Mineralogy and Petrology, 99, 249–256.

——— (1988b) Thermodynamic projection and extrapolation of high-variance mineral assemblages. Contributions to Mineralogy and Petrology, 98, 346–351.

——— (1989) Petrologic determination of metamorphic pressure-temperature-time paths. In F.S. Spear and S.M. Peacock, Eds., Metamorphic pressure-temperature-time paths, Short Course in Geology, 7, p. 1–55. American Geophysical Union, Washington, DC.

——— (1991) On the interpretation of peak metamorphic temperatures in light of garnet diffusion during cooling. Journal of Metamorphic Geology, 9, 379–388.

——— (1992) Inverted metamorphism, $P-T$ paths and cooling history of west-central New Hampshire: Implications for the tectonic evolution of central New England. In P. Robinson and J.B. Brady, Eds., Guidebook for field trips in the Connecticut Valley region of Massachusetts and adjacent states, vol. 2, p. 446–466. Department of Geology and Geophysics, University of Massachusetts, Amherst, Massachusetts.

——— (1993) Inverted metamorphism, *P-T* paths and tectonic history of west-central New Hampshire. Field Trip Guidebook for the northeastern United States: Annual Meeting of the Geological Society of America, Boston, Massachusetts, 1, D28–D33.

Spear, F.S., and Cheney, J.T. (1989) A petrogenetic grid for pelitic schists in the system SiO_2-Al_2O_3-FeO-MgO-K_2O-H_2O. Contributions to Mineralogy and Petrology, 101, 149–164.

Spear, F.S., and Florence, F.P. (1992) Thermobarometry in granulites: Pitfalls and new approaches. Journal of Precambrian Research, 55, 209–241.

Spear, F.S., Hickmott, D.D., and Selverstone, J. (1990a) Metamorphic consequences of thrust emplacement, Fall Mountain, New Hampshire. Geological Society of American Bulletin, 102, 1344–1360.

Spear, F.S., Paetzold, S.U., and Kohn, M.J. (1990b) Inverted metamorphism in west-central New Hampshire: Implications for tectonics in the Acadian Orogeny. Eos, 71, 1663.

Spear, F.S., Lin, H., Kohn, M.J., and Paetzold, S.U. (1993) Inverted metamorphism across the Bronson Hill anticlinorium, west-central New Hampshire. Geological Society of America Abstracts with Program, 25, A424.

Thompson, J.B., Jr., and Rosenfeld, J.L. (1979) Reinterpretation of nappes in the Bellows Falls–Brattleboro area, New Hampshire, Vermont. In J.W. Skehan and P.H. Osberg, Eds., The Caledonides in the USA: Geological excursions in the northeast Appalachians, p. 117–121. Weston Observatory, Weston, Massachusetts.

Thompson, J.B., Jr., Robinson, P., Clifford, T.N., and Trask, N.J. (1968) Nappes and gneiss domes in west-central New England. In E-an Zen, W.S. White, J.B. Hadley, and J.B. Thompson, Jr., Eds., Studies of Appalachian geology, northern and maritime, p. 203–218. Wiley, New York.

Thompson, P.J. (1985) Stratigraphy and structure of the Monadnock quadrangle, New Hampshire. Ph.D. dissertation, University of Massachusetts, Amherst, Massachusetts.

——— (1988) Stratigraphy and structure of the Monadnock quadrangle, New Hampshire. In W.A. Bothner, Ed., Guidebook for field trips in southwestern New Hampshire, southeastern Vermont, and north-central Massachusetts, p. 136–163. New England Intercollegiate Geological Conference, 80th meeting, Keene, New Hampshire.

Xu, G.W., Will, T.M., and Powell, R. (1994) A calculated petrogenetic grid for the system K_2O-FeO-MgO-Al_2O_3-SiO_2-H_2O, with particular reference to contact-metamorphosed pelites. Journal of Metamorphic Geology, 12, 99–119.